(30) Vermeer, P.; Meijer, J.; Brandsma, L. *Recl. Trav. Chim. Pays-Bas* **1975**, *94*, 112. Tadema, G.; Vermeer, P.; Meijer, J.; Brandsma, L. *Ibid.* **1976**, *95*, 66. Vermeer, P.; Westmijze, H.; Kleijn, H.; van Dijck, L. A. *Ibid.* **1978**, *97*, 56. Tadema, G.; Everhardus, R. H.; Westmijze, H.; Vermeer, P. *Tetrahedron Lett.* **1978**, 3935.
(31) Luche, J. L.; Barreiro, E.; Dollat, J. M.; Crabbé, P. *Tetrahedron Lett.* **1975**, 4615. Descoins, C.; Henrick, C. A.; Siddall, J. B. *Ibid.* **1972**, 3777. Moreau, J. L.; Gaudemar, M. *J. Organomet. Chem.* **1976**, *108*, 159. Crabbé, P.; Carpio, H. *J. Chem. Soc., Chem. Commun.* **1972**, 904. Crabbé, P.; Barreiro, E.; Dollat, J.-M.; Luche, J. L. *Ibid.* **1976**, 183. Rona, P.; Crabbé, P. *J. Am. Chem. Soc.* **1969**, *91*, 3289. Landor, P. D.; Landor, S. R. *J. Chem. Soc., Perkin Trans. 1* **1973**, 1347.
(32) Brikmeyer, R. S.; Macdonald, T. L. *J. Chem. Soc., Chem. Commun.* **1978**, 876. For a related system, see: Kleijn, H.; Westmijze, H.; Kruithof, K.; Vermeer, P. *Recl. Trav. Chim. Pays-Bas* **1979**, *98*, 27.
(33) (a) Pasto, D. J.; Shults, R. H.; McGrath, J. A.; Waterhouse, A. *J. Org. Chem.* **1978**, *43*, 1382. (b) Pasto, D. J.; Chou, S-K.; Waterhouse, A.; Shults, R. H.; Hennlon, G. F. *Ibid.* **1978**, *43*, 1385. (c) Gore, J.; Roumestant, M. L. *Tetrahedron Lett.* **1970**, 891. (d) Bush, C. N.; Applequist, D. E. *J. Org. Chem.* **1977**, *42*, 1076. (e) Jacobs, T. L.; Meyers, R. A. *J. Am. Chem. Soc.* **1964**, *86*, 5244; **1967**, *89*, 6177.
(34) Although it is of interest to examine the reaction of 3-chloro-3-methyl-1-butene with $RCu{\cdot}BF_3$, it is very difficult to prepare the chloride in pure form.
(35) Steinberg, H. "Organoboron Chemistry", Vol. 1; Interscience: New York, 1964; p 793.
(36) Felkin, H.; Swierczewski, G. *Tetrahedron Lett.* **1972**, 1433. Felkin, H.; Costa, E. J.; Swierczewski, G. *J. Organomet. Chem.* **1977**, *134*, 265. Buckwalter, B. L.; Burfitt, I. R.; Felkin, H.; J-Goudket, M.; Naemura, K.; Salomon, M. F.; Wenkert, E.; Wovkulich, P. M. *J. Am. Chem. Soc.* **1978**, *100*, 6445.
(37) Stork, G.; Kreft III, A. F. *J. Am. Chem. Soc.* **1977**, *99*, 3850, 3851. Cane, D. E.; Murthy, P. P. N. *Ibid.* **1977**, *99*, 8327. Magid, R. M.; Fruchey, O. S. *Ibid.* **1977**, *99*, 8368. Ikota, N.; Ganem, B. *Ibid.* **1978**, *100*, 351. Dobbie, A. A.; Overton, K. H. *J. Chem. Soc., Chem. Commun.* **1977**, 722.
(38) For importance of the stereochemistry of starting materials, see: Crabbé, P.; Dollat, J-M.; Gallina, J.; Luche, J.-L.; Velarde, E.; Maddox, M. L.; Tökes, L. *J. Chem. Soc., Perkin Trans. 1* **1978**, 730.
(39) For the stereochemistry of $S_N2'$ reaction of metal hydrides, see: Jefford, C. W.; Sweeney, A.; Delay, F. *Helv. Chim. Acta* **1972**, *55*, 2214.
(40) Booth, H. S.; Martin, D. R. "Boron Trifluoride and Its Derivatives"; Wiley: New York, 1949; p 61.
(41) Chambers, R. D.; Clark, H. C.; Willis, C. J. *J. Am. Chem. Soc.* **1960**, *82*, 5298. *Proc. Chem. Soc., London* **1960**, 114.
(42) Brauer, D. J.; Bürger, H.; Pawelke, G. *Inorg. Chem.* **1977**, *16*, 2305.
(43) Schmid, G. *Angew. Chem., Int. Ed. Engl.* **1970**, *9*, 819.
(44) For review articles, see: Tochtermann, W. *Angew. Chem., Int. Ed. Engl.* **1966**, *5*, 351. Wittig, G. *Q. Rev., Chem. Soc.* **1966**, 191. Negishi, E. *J. Organomet. Chem.* **1976**, *108*, 281.
(45) Yamamoto, Y.; Yatagai, H.; Maruyama, K.; Sonoda, A.; Murahashi, S-I. *Bull. Chem. Soc. Jpn.* **1977**, *50*, 3427.
(46) Miyaura, N.; Itoh, M.; Suzuki, A. *Bull. Chem. Soc. Jpn.* **1977**, *50*, 2199. For copper tetraarylborates via the cation exchange reaction, see: Nesmeyanov, A. N.; Sazonova, V. A.; Liberman, G. S.; Yemelyanova, L. I. *Izv. Akad. Nauk SSSR, Otd. Khim. Nauk* **1955**, 48.
(47) Cotton, F. A.; Wilkinson, G. "Advanced Inorganic Chemistry. A Comprehensive Text"; Interscience: New York, 1966; p 895.
(48) Onak, T. "Organoborane Chemistry"; Academic Press: New York, 1975; p 19.
(49) Previously we reported that considerable amounts of *n*-BuOH were obtained under this condition.[1a] However, detailed investigation revealed that most of the *n*-BuOH had its origin in lithium butylate present in *n*-BuLi as an impurity. Use of *n*-BuLi stored for long periods increased the formation of the *n*-BuOH, presumably because of the slow oxidation of *n*-BuLi by air: Panek, E. J.; Kaiser, L. R.; Whitesides, G. M. *J. Am. Chem. Soc.* **1977**, *99*, 3708.
(50) Since the complex is considerably stable, the structural information is obtained without difficulties and will be published soon. This is the first example of a stable alkenylcopper–trialkylborane ate complex.[46]
(51) Detailed studies concerning these complexes will be published elsewhere by H. Yatagai.
(52) Hatch, L. F.; Gardner, P. D.; Gilbert, R. E. *J. Am. Chem. Soc.* **1959**, *81*, 5943.
(53) (a) "Organic Syntheses", Collect Vol. V; Wiley: New York, 1973; p 859. (b) Gilman, H.; Morton Jr., J. W. *Org. React.* **1954**, *8*, 258. (c) Reference 53a, p 762.
(54) Gilman, H.; Hauben, A. H. *J. Am. Chem. Soc.* **1944**, *66*, 1515.
(55) Watson, S. C.; Eastham, J. F. *J. Organomet. Chem.* **1967**, *9*, 165.
(56) Posner, G. H.; Whitten, C. E.; Sterling, J. J. *J. Am. Chem. Soc.* **1973**, *95*, 7788.
(57) Brown, H. C. "Organic Syntheses via Boranes"; Wiley-Interscience: New York, 1975.
(58) *Org. Synth.* **1974**, *54*, 63.
(59) Stepanova, O. S.; Ganin, E. V. *Ukr. Khim. Zh.* **1977**, *43*, 168.
(60) Mori, K. *Tetrahedron* **1974**, *30*, 3807.
(61) Bokadia, M. M.; Brown, B. R.; Cobern, D.; Roberts, A.; Somerfield, G. A. *J. Chem. Soc.* **1962**, 1658.
(62) Normant, J. *Bull. Soc. Chim. Fr.* **1963**, 1888.
(63) Bateman, L.; Cunneen, J. I. *J. Chem. Soc.* **1951**, 2289.
(64) Levina, R. Y.; Skvarchenko, R.; Ushakova, T. M. *Zh. Obshch. Khim.* **1956**, *26*, 398.
(65) Bingham, A. J.; Dyall, L. K.; Norman, R. O.; Thomas, C. B. *J. Chem. Soc. C* **1970**, 1879.
(66) Goering, H. L.; Neritt, T. D.; Silversmith, E. F. *J. Am. Chem. Soc.* **1955**, *77*, 4042.
(67) Crossley, A. W.; Ronouf, N. *J. Am Chem. Soc.* **1915**, *37*, 602.
(68) Frank, R. L.; Hal Jr., H. K. *J. Am. Chem. Soc.* **1950**, *72*, 1645.
(69) Nystrom, R. F.; Borwn, W. G. *J. Am. Chem. Soc.* **1947**, *69*, 1197.
(70) Goering, H. L.; Blanchard, J. P. *J. Am. Chem. Soc.* **1954**, *76*, 5405.
(71) Macbeth, A. K.; Mills, J. A. *J. Chem. Soc.* **1949**, 2646.
(72) Liberman, A. L.; Vasina, T. V. *Neftekhimiya* **1962**, *2*, 129.
(73) Kiselev, A. V.; Migunova, I. A.; Khudyaknov, V. L.; Yashin, Y. I. *Zh. Fiz. Khim.* **1966**, *40*, 2910.
(74) Brown, H. C.; Scouten, C. G.; Liotta, R. *J. Am. Chem. Soc.* **1979**, *101*, 96.

# Tunneling Model for Hydrogen Abstraction Reactions in Low-Temperature Solids. Applications to Reactions in Alcohol Glasses and Acetonitrile Crystals[1]

**Robert J. Le Roy,*[2] Hisao Murai,[3,4] and Ffrancon Williams[3]**

*Contribution from the Guelph-Waterloo Centre for Graduate Work in Chemistry, University of Waterloo, Waterloo, Ontario, Canada N2L 3G1, and the Department of Chemistry, University of Tennessee, Knoxville, Tennessee 37916.*
*Received August 2, 1979*

**Abstract:** A simple and internally consistent quantitative model for hydrogen-abstraction reactions in low-temperature solids, which implicitly incorporates zero point energy effects which allow for finite reaction rates at $T = 0$ K, is derived and applied to new measurements of H-abstraction rate constants by methyl radicals in methanol and ethanol glasses at $T = 13$–99 K and in acetonitrile and methyl isocyanide crystals at 69–128 K. Nonlinear least-squares fits of the model to the experimental data yield effective one-dimensional barriers to reaction whose heights are virtually independent of the analytic form used for the potential energy barrier, and are somewhat larger than the activation energies measured for the corresponding reactions in the gas phase. This model predicts that values of the isotopic rate constant ratio $k_H/k_D$ will be larger than $10^{12}$ at $T = 0$ K.

Quantum-mechanical tunneling has long been believed to make a dominant contribution to the rates of many chemical reactions at low temperatures.[5,6] However, it is only relatively recently that convincing experimental evidence of this behavior has begun to appear. In most studies,[7-17] the evidence that the reactions considered proceeded mainly by tunneling consisted of (1) pronounced curvature in Arrhenius plots, (2) anomalously small activation energies, and (3) anomalously large[10,14]

0002-7863/80/1502-2325$01.00/0 

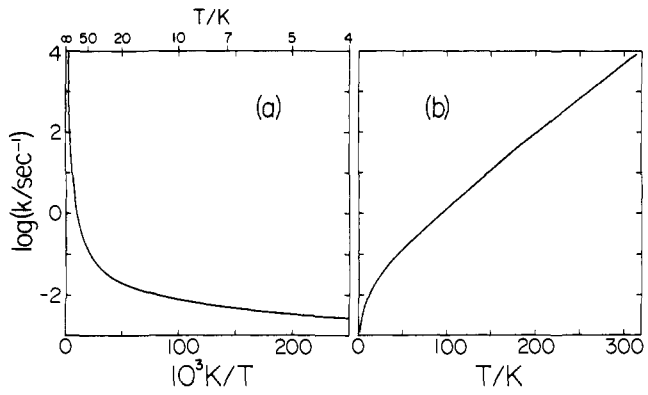


Figure 1. Hydrogen tunneling reaction rate constants calculated using the "traditional approach" from a symmetric Eckart barrier of Brunton et al.[13] for which $V_0$ = 13.8 kcal/mol and $a_1$ = 0.309 Å.

or small[17] isotope effects. For example, Sprague and Williams[7] found that H-atom abstraction by methyl radicals in γ-irradiated acetonitrile crystals at 77–87 K had an apparent activation energy of only ca. 1.4 kcal/mol, a value much smaller than the 10.1 (±0.5) kcal/mol determined[18] from room temperature gas-phase studies of this reaction. Moreover, the analogous D-atom abstraction was too slow to be detected at these temperatures,[7,14] and Sprague[14] showed that at 77 K the deuterium isotope effect gives rise to a rate constant ratio $k_H/k_D$ in excess of 28 000, a value some 20 times larger than the maximum isotope effect expected in the absence of tunneling. Quantitative justification for attributing such effects to tunneling was provided by the excellent agreement of experimental rate constants and their temperature and isotope dependence with the calculated transmission rates for thermal distributions of free particles colliding with potential energy barriers of realistic height and width.[8,9,12,13,15]

An even more dramatic tunneling effect is the approximate temperature independence displayed by some rate constants at very low temperatures (say, $T \lesssim 30$ K).[19-23] This behavior is particularly intriguing since it implies the existence of nonzero reaction rates even at $T = 0$ K. It is widely believed that this type of behavior was predicted in 1935 by Bell's[5] treatment of tunneling through truncated parabolic barriers. However, that prediction is an artifice of Bell's use of an approximate barrier permeability formula which predicts a finite transmission probability for particles impinging on a truncated parabolic barrier at zero kinetic energy. A fully quantum-mechanical treatment of this problem shows that this is incorrect,[24] and that, as with smooth barriers (such as the familiar Eckart function[25]) which are infinitely broad at the base, the transmission probability for a truncated parabolic barrier actually approaches zero at zero incident energy. Thus, the (exact) thermally averaged barrier transmission rate for a truncated parabolic barrier also approaches zero as $T \rightarrow 0$ K. While use of asymmetric exothermic potential barriers rather than symmetric ones does enchance the predicted transmission rates for low temperatures,[17,26] the existence of a finite rate constant at 0 K is still not explained by any model which involves a thermal distribution of particles impinging on one of these "traditional" model potential barriers.

There are two ways in which the usual model of these low-temperature reactions as the transmission of a stream of particles through a potential-energy barrier can be modified in order to take account of this limiting temperature independence of the predicted rate constants. The first is to use model barriers of finite range which go to zero smoothly at some finite distance[27] and do not have the abrupt discontinuities in slope which make the (exact) tunneling probability for a truncated parabolic barrier become zero at zero incident energy. However, in this approach there would be no natural way to explain the source of the incident flux in this 0 K limit, so this approach will not be considered further.

A much more plausible solution to this problem was suggested 20 years ago by Goldanskii,[28] who pointed out that, if the Boltzmann continuum of reagent energies was replaced by a discrete set of initial energies associated with the vibrational motion of the reagents, the rate constant at absolute zero would correspond simply to tunneling at the (nonzero) incident energy corresponding to the zero-point level. This explanation has been invoked for rationalizing some of the recent observations of approximately temperature-independent rate constants at low temperature.[19-21] However, no detailed model of these processes which takes full account of this behavior has yet been presented. A master equation approach to the problem of reactions initiated from a discrete set of reagent levels was proposed by Cribb et al.,[29] and their method does predict nonzero rate constants at 0 K. However, the only reagent states allowed by their model are the vibrational levels of the potential well representing the initial states of the system. This does not provide a very realistic picture of the reagents in low-temperature solids where internal rotation and vibrations of the matrix blur these discrete initial states and provide a quasi-continuous range of incident energies. The present paper therefore presents a detailed model of intermolecular hydrogen atom abstraction reactions under these conditions, which implicitly incorporates the zero point energy effect predicted by Goldanskii.[28] Some new rate data for H-atom abstraction by methyl radicals in methanol and ethanol glasses and in acetonitrile and methyl isocyanide crystals are presented, and the model is tested for its ability to fully account for the data for the five systems considered.

Before proceeding further, it is perhaps important to point out that examination of an Arrhenius plot is not a reliable way for determining whether the rate constants for a given reaction approach a finite limit at $T = 0$ K. This fact is demonstrated by Figure 1, where rate constants for $T$ = 4–300 K, calculated using one of the symmetric Eckart barriers considered by Brunton et al.,[13] are plotted both in the traditional Arrhenius form vs. $1/T$ and vs. $T$ itself. Figure 1b clearly shows that these predicted rate constants approach zero at $T \rightarrow 0$ K. However, the distortion of the temperature scale in the traditional Arrhenius plot of Figure 1a makes these same rate constants appear to be approaching a constant by around liquid helium temperature (4.2 K). It is therefore clear that the characteristic behavior of rate constants at very low temperatures is much more readily ascertained from plots of the rate constant (or its logarithm[30]) vs. some positive power of $T$ than from the ubiquitous Arrhenius plot.[31]

## Theory

The reactions considered here are those involving the exothermic transfer of an atom (usually hydrogen or deuterium) between two neighbors in a solid matrix (either a crystal or a glass):

$$R\text{-}H + R'\cdot \rightarrow R\cdot + R'\text{-}H \qquad (1)$$

where the reagent R′· is typically a methyl radical and R–H is the host species forming the matrix. Since the reagents and products are frozen into fixed sites in the matrix, it should be a fairly good approximation to treat such reactions as the unimolecular transfer of the atom between the two wells of a double minimum potential such as that shown in Figure 2b. Species to the left of the barrier maximum are classified as reagents and those to the right as products. Justifications for modeling a chemical reaction by this type of simple one-dimensional reaction coordinate have been presented by others[32-37] and will not be repeated here. However, this type of approximation does seem particularly reasonable in the present

situation where the partners of the atom being transferred are held at fixed positions by the matrix.

The temperatures considered here all correspond to thermal energies which are much smaller than both the reagent barrier height and the reaction exothermicity. This justifies the neglect of back reactions, since once the product R′-H species is formed, the reverse reaction is sufficiently slow that it will not occur before the species thermally relaxes to a lower energy state which either lies below the threshold for back reaction or corresponds to a very much smaller specific rate constant. The assumption that effects due to back reactions may be neglected is used throughout the present work, including those cases in which the barrier for an exothermic reaction is approximated by a symmetric potential energy function.

### Critical Summary of the "Traditional" Approach

In a recent paper, Cribb et al.[29] presented a nice derivation of the quantum-corrected transition-state theory for one-dimensional reactions, as applied to the double-well problem. The following discussion generalizes and expands upon their approach in order to incorporate important physical features of the reactions of interest here. As a starting point, the rate constant is written as

$$k(T) = \sum_E k(E)g(E)e^{-E/k_BT} \Big/ \sum_E g(E)e^{-E/k_BT} \quad (2)$$

where $g(E)$ is the total degeneracy of reagent energy level $E$, $k(E)$ is the corresponding specific rate constant, $k_B$ is Boltzmann's constant, and the sum is over all possible reagent energies. The specific rate constant $k(E)$ may in general be written as the product of a frequency factor, $\nu(E)$ $s^{-1}$, times the barrier permeability at energy $E$, $P(E)$: $k(E) = \nu(E)P(E)$.[38] For the case of a simple continuum of initial energies, the degeneracy factor $g(E)$ is replaced by the density of states $\rho(E)$ and eq 2 becomes

$$k(T) = \int_0^\infty dE\, \nu(E)P(E)\rho(E)e^{-E/k_BT} \Big/ \int_0^\infty dE\, \rho(E)e^{-E/k_BT} \quad (3)$$

Cribb et al.[29] showed that, if the initial states correspond to the vibrational levels of *any* single-minimum potential and the frequency factor $\nu(E)$ is the classical vibrational frequency associated with this vibrational motion, then $\rho(E) = 1/h\nu(E)$. Introduction of the harmonic oscillator approximation that $\nu(E) = \bar{\nu}$ is independent of energy then yields the simple rate constant expression used in a number of tunneling-model analyses of experimental data:[8,9,12,13,15,21,23,24]

$$k(T) = (A/k_BT) \int_0^\infty dE\, P(E)e^{-E/k_BT} \quad (4)$$

where $A = \bar{\nu}$.

In a number of studies,[8,9,12,13,15] rate constants calculated from eq 4 using the permeabilities $P(E)$ for realistic model potential barriers were able to accurately reproduce the experimental data over the full range of temperature for which results were available. However, the increasing inadequacy of its predictions in cases where experimental results are available at very low temperatures ($T \lesssim 30$ K)[19-23] warns of a serious weakness in this model. A more subtle sign of weakness is the rather curious (in retrospect) conclusion of ref 9 that, in the very limited temperature range $T = 77$–$87$ K, the analysis was extremely sensitive to the functional form of the model barrier (i.e., Gaussian vs. Eckart vs. truncated parabola). In the following, we present an improved version of this model which takes better account of the actual nature of the reacting system and implicitly allows for the existence of nonzero reaction rates of 0 K.

### Improved Model for Abstraction Reactions in Solids

As pointed out in ref 9 and 21, a serious inconsistency of the above model is its use of the stretching frequency of the quantized R-H vibration to define the $A$ factor in eq 6 while the integral over energy assumes a continuous Boltzmann distribution extending down to $E = 0$. In the present approach this inconsistency is removed by partitioning the total energy, $E = E_v + E_c$, into a term associated with the stretching of the R-H bond, $E_v$, plus a term $E_c$ associated with all other types of motion (internal rotation, lattice vibrations, etc.) which can contribute energy to motion along the reaction path. The former is of course quantized, while the spectrum of allowed values of $E_c$ is assumed to be a continuum for which the associated density of states $\rho(E_c)$ does not depend on the vibrational quantum number $v$.

As in the previous model, the reaction is assumed to be initiated by the large amplitude asymmetric stretching of the R-H bond, so the frequency factor appearing in the specific rate constant is simply the frequency of this motion. However, geometric considerations such as the orientation of the R-H bond relative to the R′· scavenger may mean that only a fraction of the momentum associated with this stretching contributes to motion along the reaction coordinate. It is therefore necessary to distinguish between the total vibrational energy of the bond being broken, $\epsilon_v$, and that portion of it which may contribute to motion along the reaction path, $E_v$. Since the two are related solely by a geometric factor, it is clear that $E_v/\epsilon_v \leq 1$ is a nonnegative constant which is independent both of $v$ and of the mass of the atom being transferred.

Application of this energy partitioning to eq 2 yields the basic rate constant expression associated with the present model:

$$k(T) = \sum_v \nu(v)e^{-\epsilon_v/k_BT} \times \left( \int_0^\infty dE_c\, P(E_v + E_c)\, \rho(E_c)e^{-E_c/k_BT} \right) \times \left\{ \sum_v e^{-\epsilon_v/k_BT} \left( \int_0^\infty dE_c\, \rho(E_c)e^{-E_c/k_BT} \right) \right\}^{-1} \quad (5)$$

In the absence of a detailed knowledge of the distribution of energies $E_c$, it is convenient to introduce the approximation that $\rho(E_c)$ is a constant. Combining this with the harmonic oscillator approximation, which implies that $\nu(v) = \bar{\nu}$ is a constant and hence that

$$\epsilon_v = (2v + 1)\epsilon_0 = (v + \tfrac{1}{2})h\bar{\nu}$$
$$E_v = (2v + 1)E_0 \quad (6)$$

for $v = 0, 1, 2$, etc., then reduces eq 5 to the form used in the analyses reported below:

$$k(T) = (A/k_BT)[1 - e^{-h\bar{\nu}/k_BT}] \times \left( \int_{E_0}^\infty dE\, F(E)P(E)e^{-(E-E_0)/k_BT} \right) \quad (7)$$

where again $A = \bar{\nu}$ and

$$F(E) = \sum_{v(E_v \leq E)} e^{-2v(\epsilon_0 - E_0)/k_BT} \quad (8)$$

The concomitant expression for the apparent Arrhenius activation energy, $E_A \equiv k_BT^2\, \partial \ln (k)/\partial T$, is readily obtained by differentiation of eq 7:

$$E_A = -k_BT - h\bar{\nu}/(e^{h\bar{\nu}/k_BT} - 1) + \left( \int_{E_0}^\infty dE[(E - E_0)F(E) + G(E)]P(E)e^{-(E-E_0)/k_BT} \right) \times \left( \int_{E_0}^\infty dE\, F(E)P(E)e^{-(E-E_0)/k_BT} \right)^{-1} \quad (9)$$

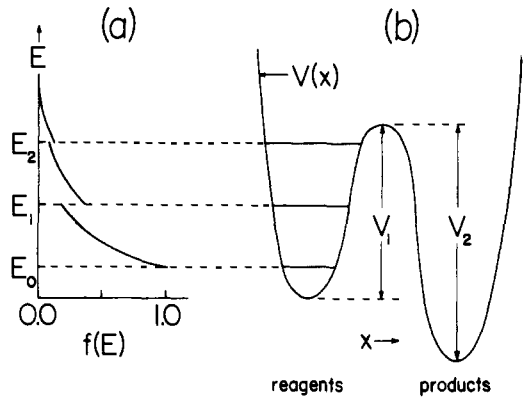


**Figure 2.** (a) Effective population distribution function $f(E) = F(E) \cdot e^{-(E-E_0)/k_BT}$ from eq 7 for the case $E_0 = \epsilon_0$. (b) Sketch of potential-energy curve along the reaction path.

where

$$G(E) = \sum_{v(E_v \leq E)} 2v(\epsilon_0 - E_0)e^{-2v(\epsilon_0-E_0)/k_BT} \qquad (10)$$

In the simple case when $E_0 = \epsilon_0$ (*i.e., all* of the reagent vibrational energy contributes to motion along the reaction path, $F(E)$ is simply the number of reagent vibrational levels for which the energy contributing to motion along the reaction path, $E_v$, is less than $E$. For this case, the schematic plot of the effective population distribution function $f(E) = F(E) \cdot e^{-(E-E_0)/k_BT}$ shown in Figure 2a illustrates the essential features of the present model. It clearly implies that the lowest accessible reagent energy lies $E_0$ above the base of the barrier to reaction, at a point where the barrier permeability is nonzero. Thus, the reaction may proceed at a finite rate even at 0 K when only this zero-point level is populated.

The other extreme case for the present model corresponds to the limit when $E_0 \to 0$, i.e., when virtually none of the reagent vibrational energy contributes to motion along the reaction path; in this limit eq 7 reduces to the traditional tunneling model rate constant expression of eq 4. Thus, the present model provides a sound physical reason for setting the $A$ factor of eq 4 equal to the stretching frequency of the bond being broken by the reaction.

It is important to realize that the essential characteristics of the present model are in no way dependent on either the approximation that $\rho(E_c)$ is a constant or on the harmonic approximation represented by eq 6 and the assumption that $\nu(v) = \bar{\nu}$. Removal of the harmonic approximation simply means that (1) the harmonic vibrational partition function $[1 - e^{-h\bar{\nu}/k_BT}]^{-1}$ appearing in eq 7 and 9 must be replaced by a direct sum for the actual vibrational energies, (2) the quantity $2v(\epsilon_0 - E_0)$ appearing in eq 8 and 10 must be replaced by $[(\epsilon_v - \epsilon_0) - (E_v - E_0)]$, and (3) the (at most weak) dependence of $\nu(v)$ on the vibrational state will require minor additional changes in the definitions of $F(E)$ and $G(E)$. While the resulting rate-constant expression would be more complex, its basic properties would be essentially the same as those of eq 7. In practice, however, the $v = 0$ level is usually the only one which contributes significantly to reaction at low temperatures, so deviations from harmonic behavior are of little real importance. Similarly, if a realistic estimate of $\rho(E_c)$ is available, its use in eq 5 would require the integral in the denominator to be evaluated numerically too, but would neither make the calculations significantly more complex nor change the main features of the resulting $k(T)$ values.

### Fitting the Model to Experimental Data

Since the frequency $\bar{\nu}$ and the total vibrational energy $\epsilon_v$, are known properties of the reagent R-H,[39] rate constants calculated from eq 7 depend only on the values of $E_0$ and of the parameters characterizing the potential-energy barrier which defines the permeability function $P(E)$. For Eckart barriers these permeabilities are known analytically,[25] while for any other barrier shape they may be readily calculated numerically.[9,24] The analysis reported here involves determination of those values of $E_0$ and the barrier parameters for which the calculated rate constants agree best with experiment. This is accomplished by performing nonlinear least-squares fits[40] of rate constants calculated from eq 7, to the experimental data. As in any least-squares fitting procedure, one is attempting to minimize the weighted sum of squares of deviations

$$\chi^2 = \sum_{i=1}^{N_d} [Y_i(\text{exp}) - Y_i(\mathbf{p})]^2/u_i^2 \qquad (11)$$

where $N_d$ is the number of data being fitted, $Y_i(\text{exp})$ is the $i$th experimental datum, $Y_i(\mathbf{p})$ is the value of it calculated from a model defined by the trial parameters $\mathbf{p} = \{p_1, p_2, \ldots\}$, and $(u_i)^2$ is the sum of the squared uncertainties in the calculated and observed quantities (assuming the two to be uncorrelated). In the present case, the uncertainty in the calculated rate constants implied by the model may be made arbitrarily small, so $u_i$ is attributed solely to experimental uncertainty.

If an estimated uncertainty is known for each of the experimental rate constants, the rate constant itself may be used as the dependent variable $Y_i$ in the $\chi^2$ minimization procedure. While such individual estimates are not available for the cases considered here, to a very good approximation their *relative* uncertainties are believed to be the same for all of the measured rate constants for a given system. The present analysis therefore identified the logarithm of the rate constant,[30] $Y_i \equiv \log [k(T_i)]$, as the dependent variable in the fits and set all of the associated statistical weights $(u_i)^{-2} = 1$. The quality of fit is then indicated by the value of the standard deviation $\sigma \equiv [\min(\chi^2)/(N_d - N_p)]^{1/2}$ where $N_p$ is the number of parameters being varied.

Most efficient $\chi^2$ minimization procedures[40] require evaluation of the partial derivatives $\partial Y_i(\mathbf{p})/\partial p_j$ of each calculated datum with respect to each of the parameters being varied. For models based on potential barriers for which the exact permeability $P(E)$ is a known analytic function of the barrier parameters, exact derivatives of $k(T)$ with respect to $p_j$ are readily obtained from eq 7 by simply replacing $P(E)$ in the integral by the analogous known quantity $\partial P(E)/\partial p_j$. For other types of potentials, these derivatives are readily estimated using divided differences: $\partial Y_i(\mathbf{p})/\partial p_j \approx \Delta Y_i(\mathbf{p})/\Delta p_j$. In this second case, care must be taken that the increment $\Delta p_j$ is both sufficiently small that the secant approximation provides a reliable estimate of the actual derivative and sufficiently large that evaluation of the difference in the numerator does not cancel all the significant digits of the calculated rate constants. In the present work, these restrictions were met by choosing values of $\Delta p_j$ for which the corresponding average change in $Y_i(\mathbf{p}) = \log [k(T_i)]$ was 0.02 (i.e., which gave rise to a 5% change in the calculated $k(T_i)$ values).

The "best fit" of a given model to a set of experimental data would of course correspond to the global minimum of $\chi^2$ as a function of the potential barrier parameters $\mathbf{p}$. As in any nonlinear least-squares fit, this $\chi^2$ hypersurface may in principle have a number of local minima, and there is no rigorous way of assuring that a minimum to which the fitting procedure converges is indeed this global minimum. However, if fits starting from widely different trial parameters converge on the same point, it should be clear that there are no false local minima within the range of parameters surveyed. Throughout the present work, no such false minima were encountered, so it seems that the type of fitting procedure used here can reliably yield unique optimized potential parameters for any reasonable model barrier.

**Table I.** Known Properties of the Reaction Systems[d]

| matrix | $N_d$ | $\Delta T$/K | $\bar{\nu}$/s$^{-1}$ [a] | $\epsilon_0$/kcal mol$^{-1}$ [b] | $-\Delta H$/kcal mol$^{-1}$ [c] | $E_A$(gas)/kcal mol$^{-1}$ [c] |
|---|---|---|---|---|---|---|
| methanol | 30 | 14.8-89.5 | $8.8 \times 10^{13}$ | 4.196 | 8.1 | 10.0 (±1.0) |
| ethanol | 31 | 13.0-99.2 | $8.8 \times 10^{13}$ | 4.196 | 10.9 | 9.7 (±1.0) |
| acetonitrile I | 35 | 69.2-113.2 | $8.9 \times 10^{13}$ | 4.244 | 19.9 | 10.1 (±1.0) |
| acetonitrile II | 31 | 77.3-128.2 | $8.9 \times 10^{13}$ | 4.244 | 19.9 | 10.1 (±1.0) |
| methyl isocyanide | 19 | 77.3-125.8 | $8.9 \times 10^{13}$ | 4.244 | | |

[a] T. Shimanouchi, "Tables of Molecular Vibrational Frequencies", *Natl. Stand. Ref. Data Ser., Natl. Bur. Stand.*, **No. 6** (1967); **No. 11** (1967); **No. 17** (1968). [b] Defined as $h\bar{\nu}/2$. [c] J. A. Kerr and J. J. Parsonage, "Evaluated Kinetic Data on Gas-Phase Hydrogen Transfer Reactions," Butterworths, London, 1976. [d] $\Delta T$ is the temperature range spanned by the $N_d$ experimental rate constants.

### Potential Models Used in the Analysis

In the fits reported below, four different model potentials are considered: symmetric and asymmetric Eckart barriers

$$V_E = [(V_1)^{1/2} + (V_2)^{1/2}]^2/4 \cosh^2(x/a_1) - (V_2 - V_1)e^{x/a_1}/2 \cosh(x/a_1) \quad (12)$$

and symmetric and asymmetric Gaussian barriers

$$V_G(x) = V_1 e^{-(x/a_1)^2} \quad \text{for } x \leq 0$$
$$= V_2 e^{-(x/a_2)^2} - (V_2 - V_1) \quad \text{for } x > 0 \quad (13)$$

Here $V_1$ is the barrier height to reagents and $V_2$ is the barrier height for the corresponding back reaction, and the two Gaussian barrier width parameters $a_1$ and $a_2$ are interrelated by the requirement $a_2 = a_1\sqrt{V_2/V_1}$ which ensures that the second derivative of an asymmetric Gaussian barrier is continuous at $x = 0$. Since the reaction exothermicity $\Delta V$ is a fixed (and usually known) quantity, it should not be treated as a variable in the analysis, and, if the difference between reagent and product zero-point energies is ignored, one can write $V_2 = V_1 + \Delta V$. As a result, there are only two free parameters characterizing each of the four barriers mentioned: the reagent barrier height $V_1$ and the width parameter $a_1$.

In the past, fits of calculated rate constants to experimental data using the simple tunneling model of eq 4 have also been performed using barriers defined in terms of truncated parabola or Lorentzian functions,[9,13,23] and it is clear that any number of analytic functions could be devised for representing such barriers. However, if the present model for these processes is correct, the quality of the fit should not depend too much on the precise analytic form of the potential-energy function. Indeed, the apparent sensitivity to the functional form of the potential-energy barrier reported in some earlier studies[9,13] is one indication of the inadequacy of models assuming a pure continuum of incident reagent energies. The four barrier types described above should provide enough variety to allow this model independence of the analysis to be properly tested.

### Summary by Experimental Methods and Rate Constants

**Abstraction by Methyl Radicals in Methanol and Ethanol Glasses.** The technique of methyl radical generation and the details of the kinetic measurements by EPR spectroscopy have been described previously for studies of the reaction at cryogenic temperatures in methanol glasses.[11,21] Essentially the same methods were employed in the investigation of the corresponding hydrogen transfer in ethanol glasses, the only difference being the use of a shorter exposure time (10 s) for the photochemical generation of methyl radicals. The decay of the methyl radical in ethanol was determined by monitoring the inner lines ($M_I = \pm \frac{1}{2}$) of the 1:3:3:1 spectrum. First-order rate constants were evaluated from semilogarithmic kinetic plots by the least-squares method using data points from the initial portion of the decay over a period of 5 min. As observed previously for the reaction in the methanol glass,[11,21] the first-order plots showed a slight curvature but the decay curves for different initial concentrations of the methyl radical in ethanol at the same temperature were exactly superimposable when plotted as a percentage of the initial concentration. This result excludes second-order processes, as expected for a reaction with the matrix molecules, and the hydrogen transfer is considered to obey composite first-order kinetics,[41] The correlation coefficients for the first-order plots were between 0.93 and 1.00 over the entire temperature range, with the majority of values being above 0.96. These results justify the use of a simple first-order relationship for the initial portion of the decay curve despite the slight curvature noted above. A microscopic interpretation of the composite first-order character of these hydrogen-transfer reactions in glasses has been given previously.[21]

The experimental proof that the decay of the methyl radical in ethanol glass takes place by hydrogen-atom transfer from the $\alpha$ carbon of the ethanol was obtained by following the growth of the EPR signal attributable to $CH_3\dot{C}HOD$ in the ethanol-*d* ($C_2H_5OD$) glass. This signal was observed at a field position about 10 G less than the low-field ($M_I = +\frac{3}{2}$) component of the methyl radical quartet. The rate constants calculated from $CH_3\cdot$ decay and $CH_3\dot{C}HOD$ growth at 77 K agreed within the experimental error of each determination.

The decay of methyl radicals at 77 K in a deuterated (99 atom % D) ethanol glass was slower than in $C_2H_5OH$ by a factor of about $6 \times 10^2$. To ascertain if this decay might be due to hydrogen atom transfer from the residual concentration of protiated molecules in the matrix, the decay was measured as a function of added $C_2H_5OD$ concentration in the range from 0.57 to 5.3 mol %. Allowing for an effective concentration of 1 mol % $C_2H_5OH$ in the neat deuterated ethanol, a plot of the rate constants vs. the combined $C_2H_5OD$ and $C_2H_5OH$ concentration yielded a smooth curve which extrapolated to a limiting rate constant for the 100% $C_2D_5OD$ system which was at least ten times lower than that obtained for the 99 atom % D material. Hence, the deuterium isotope effect in the ethanol system at 77 K corresponds to a rate constant ratio $k_H/k_D$ greater than $6 \times 10^3$.

For the five abstraction reactions discussed herein, Table I lists the number $N_d$ and temperature range $\Delta T$ for the experimental rate constants, together with the stretching frequencies $\bar{\nu}$ and associated zero-point energies $\epsilon_0 \equiv h\bar{\nu}/2$ for the C-H bonds being broken and the exothermicities $-\Delta H$ and gas-phase activation energies $E_A$(gas) reported for these systems. Tables of the experimental rate constants are presented in the supplementary material deposited with this paper. Experimental errors can result from variations in the temperature during the kinetic experiment as well as from drifts in the signal from the EPR spectrometer. From the repeatability of the data, the error (standard deviation) in the rate constant is estimated to be ±20%.

**Abstraction by Methyl Radicals in Crystalline Methyl Isocyanide and Methyl Cyanide (Acetonitrile).** The experimental techniques that were used to study the reaction in methyl isocyanide have been described.[10] Essentially, the procedure consisted of generating the methyl radical by $\gamma$-irradiation at 77 K followed by kinetic EPR measurements at the temperature of interest in the range between 77 and 126 K. Both the decay of the methyl radical and the concomitant growth of the

**Table II.** Results of Fits to Rate Constants for Abstraction in Methanol Glass

| potential form | $\sigma$ | $E_0$/kcal mol$^{-1}$ | $V_1$/kcal mol$^{-1}$ | $a_1$/Å | log [$k(T = 0)$/ s$^{-1}$] |
|---|---|---|---|---|---|
| SE | 0.110 | 4.196 | 12.25(0.24) | 0.979(0.024) | −3.70 |
| SG | 0.111 | 4.196 | 11.87(0.20) | 1.079(0.023) | −3.69 |
| AE | 0.111 | 4.196 | 11.93(0.20) | 1.197(0.028) | −3.69 |
| AG | 0.114 | 4.196 | 11.65(0.17) | 1.148(0.022) | −3.67 |
| SE | 0.238 | 0.0 | 30.05(10.00) | 0.268(0.049) | −∞ |
| SG | 0.227 | 0.0 | 16.05(3.65) | 0.455(0.058) | −∞ |
| AE | 0.203 | 0.0 | 16.17(2.61) | 0.483(0.051) | −∞ |
| AG | 0.174 | 0.0 | 10.31(0.95) | 0.660(0.036) | −∞ |

**Table III.** Results of Fits to Rate Constants for Abstraction in Ethanol Glass

| potential form | $\sigma$ | $E_0$/kcal mol$^{-1}$ | $V_1$/kcal mol$^{-1}$ | $a_1$/Å | log [$k(T = 0)$/ s$^{-1}$] |
|---|---|---|---|---|---|
| SE | 0.156 | 4.196 | 12.51(0.24) | 0.946(0.026) | −3.53 |
| SG | 0.154 | 4.196 | 12.15(0.20) | 1.039(0.023) | −3.50 |
| AE | 0.154 | 4.196 | 12.19(0.20) | 1.190(0.029) | −3.50 |
| AG | 0.156 | 4.196 | 11.93(0.17) | 1.108(0.022) | −3.46 |
| SE | 0.340 | 0.0 | 24.95(8.52) | 0.295(0.059) | −∞ |
| SG | 0.318 | 0.0 | 14.00(2.85) | 0.488(0.059) | −∞ |
| AE | 0.301 | 0.0 | 14.92(2.70) | 0.522(0.066) | −∞ |
| AG | 0.252 | 0.0 | 9.83(0.86) | 0.681(0.039) | −∞ |

**Table IV.** Results of Fits to Rate Constants for Abstraction in Crystal I of Acetonitrile

| potential | $\sigma$ | $E_0$/kcal mol$^{-1}$ | $V_1$/kcal mol$^{-1}$ | $a_1$/Å | log [$k(T = 0)$/ s$^{-1}$] |
|---|---|---|---|---|---|
| SE | 0.096 | 4.244 | 13.76(0.14) | 0.886(0.014) | −4.19 |
| SG | 0.108 | 4.244 | 13.43(0.13) | 0.966(0.014) | −4.08 |
| AE | 0.108 | 4.244 | 13.44(0.13) | 1.177(0.018) | −4.08 |
| AG | 0.123 | 4.244 | 13.19(0.12) | 1.039(0.014) | −3.97 |
| SE | 0.067 | 0.0 | 12.88(0.40) | 0.483(0.012) | −∞ |
| SG | 0.067 | 0.0 | 10.92(0.22) | 0.613(0.010) | −∞ |
| AE | 0.066 | 0.0 | 11.16(0.24) | 0.747(0.015) | −∞ |
| AG | 0.075 | 0.0 | 9.71(0.14) | 0.742(0.009) | −∞ |

·$CH_2NC$ radical were followed, the derived first-order rate constants generally agreeing with each other to 10% or better.

In contrast to the studies in alcohol glasses, where composite first-order kinetics applies, the reaction kinetics in the crystalline systems of methyl isocyanide and acetonitrile obeyed the simple first-order relation without any significant deviation for more than 90% of the reaction. Since the orientation of the reaction partners is expected to be uniform in a crystalline (or polycrystalline) substance, this result lends strong support to the idea noted above that composite first-order kinetics results from the nonhomogeneous orientation of reactants in a glassy matrix.

Acetonitrile possesses two crystalline phases with the solid-solid transition occurring at 217 K.[42] However, studies of the reaction in the temperature range from 69 to 128 K were not confined to the thermodynamically stable low-temperature phase (crystal II) since the high-temperature phase (crystal I) could be metastabilized by rapid cooling from above the transition temperature to 77 K. Therefore, studies were made on the kinetics of the reaction in each of the two solid phases, the data being treated independently since the results for the two phases at the same temperature were not in agreement. Of course, this is expected to be the case for an intermolecular solid-state reaction which is sensitive to the width of the potential barrier.

Methyl radicals were generated in the crystalline acetonitrile phases by subsequent photobleaching of acetonitrile radical anions produced by $\gamma$-irradiation. As described elsewhere,[43-45] the dimer radical anion is produced in crystal I and the monomer radical anion in crystal II. Since both these species are photosensitive to light from a tungsten filament lamp, it was possible to generate a high yield of methyl radicals almost instantaneously at any reaction temperature. This feature allowed for a greater flexibility in the study of the reaction in acetonitrile as compared to methyl isocyanide, especially at the higher temperatures.

Rate constants for hydrogen-atom abstraction from acetonitrile were derived from EPR measurements similar to those already described for methyl isocyanide, using data points for the decay of $CH_3$· and the growth of ·$CH_2CN$. Since the mechanism of methyl radical decay in the acetonitrile systems also involves a parallel first-order reaction leading to the recovery of the appropriate radical anion,[7] the experimental rate constant obtained from measurements made on the dark reaction after a short burst of intense illumination is equal to the sum of the rate constants for abstraction and recovery. However, if the sample is exposed to steady illumination such that the recovery reaction is completely and continuously reversed by the photobleaching process, then the measured rate constant refers only to the abstraction process.[7,46] In practice, the contribution due to the recovery reaction becomes very significant in the higher range of temperatures which have been studied.

An independent method of obtaining the rate constant for the abstraction reaction in the acetonitrile crystalline phases depended on following the recovery of the optical absorption band due to the radical anion.[47] From the theory of parallel first-order reactions,[48] the measured or apparent rate constant is again the sum of the rate constants for abstraction and recovery. Multiplication of this result by the fraction of the original absorption which was ultimately recovered in the ex-

**Table V.** Results of Fits to Rate Constants for Abstraction in Crystal II of Acetonitrile

| potential | $\sigma$ | $E_0$/kcal mol$^{-1}$ | $V_1$/kcal mol$^{-1}$ | $a_1$/Å | log $[k(T = 0)/$ s$^{-1}]$ |
|---|---|---|---|---|---|
| SE | 0.123 | 4.244 | 14.58(0.12) | 0.879(0.013) | −5.24 |
| SG | 0.148 | 4.244 | 14.33(0.12) | 0.950(0.014) | −5.04 |
| AE | 0.147 | 4.244 | 14.34(0.12) | 1.148(0.018) | −5.05 |
| AG | 0.177 | 4.244 | 14.15(0.12) | 1.014(0.015) | −4.86 |
| SE | 0.103 | 0.0 | 12.15(0.32) | 0.552(0.014) | −∞ |
| SG | 0.092 | 0.0 | 11.05(0.17) | 0.659(0.010) | −∞ |
| AE | 0.093 | 0.0 | 11.14(0.18) | 0.813(0.015) | −∞ |
| AG | 0.101 | 0.0 | 10.31(0.11) | 0.765(0.009) | −∞ |

**Table VI.** Results of Fits to Rate Constants for Abstraction in Crystals of Methyl Isocyanide

| potential | $\sigma$ | $E_0$/kcal mol$^{-1}$ | $V_1$/kcal mol$^{-1}$ | $a_1$/Å | log $[k(T = 0)/$ s$^{-1}]$ |
|---|---|---|---|---|---|
| SE | 0.129 | 4.244 | 14.56(0.20) | 0.862(0.019) | −4.84 |
| SG | 0.155 | 4.244 | 14.29(0.20) | 0.934(0.020) | −4.67 |
| AE | 0.154 | 4.244 | 14.30(0.20) | 1.129(0.026) | −4.68 |
| AG | 0.185 | 4.244 | 14.10(0.20) | 0.998(0.022) | −4.51 |
| SE | 0.098 | 0.0 | 12.57(0.49) | 0.523(0.018) | −∞ |
| SG | 0.088 | 0.0 | 11.21(0.26) | 0.636(0.013) | −∞ |
| AE | 0.089 | 0.0 | 11.34(0.28) | 0.781(0.020) | −∞ |
| AG | 0.100 | 0.0 | 10.33(0.18) | 0.747(0.012) | −∞ |

periment yields the rate constant for recovery, and hence the value for abstraction can be determined by difference.

The experimental techniques which were used in following the reactions by optical spectroscopy have been described.[47] Most of the studies were carried out using a specially designed optical cryostat[47c] cooled by a flow of nitrogen gas using an arrangement similar to that employed routinely for variable-temperature EPR studies. The cryostat was inserted into the sample compartment of the Cary 14 spectrophotometer and the optical cell containing the $\gamma$-irradiated acetonitrile positioned in the light beam. After the initial optical absorption had been measured, the sample was photobleached in situ and the recovery of the optical band followed at the temperature of interest. The temperature of the sample was constantly monitored during the run and could be controlled to within a fraction of a degree Kelvin.

The EPR and optical determinations of the rate constants for abstraction are in such good agreement for both crystal I and crystal II of acetonitrile that we have not differentiated between the two sets of results in the figures showing the temperature dependence of the rate constant. However, the source of the data is referenced in tables included as supplementary material.

## Results and Discussion

The results of nonlinear least-squares fits of the present model to the five sets of experimental rate constants described above are summarized in Tables II–VI. In order to ascertain the model dependence of the analysis, the fits for each case were performed using four different potential barrier shapes: symmetric Eckart (SE), symmetric Gaussian (SG), asymmetric Eckart (AE), and asymmetric Gaussian (AG). In all of these fits, the frequency parameters $\bar{\nu}$ and $A$ were held fixed at the appropriate value listed in Table I. For the first four sets of data the exothermicity of the asymmetric barriers $\Delta V \equiv V_2 - V_1$, was held fixed at the thermodynamic value given in Table I. However, since no $\Delta H$ value was available for the methyl isocyanide abstraction reaction, $\Delta V$ for this case was arbitrarily set equal to the value for the acetonitrile reaction, 19.9 kcal mol$^{-1}$. The overall quality of each fit is indicated by the value of the standard error, $\sigma$, which has units log $[k/\text{s}^{-1}]$. The statistical uncertainties in the fitted values of $V_1$ and $a_1$ for each case, given in parentheses, correspond to a 95% confidence limit (approximately 2 standard errors). The last column of each row of these tables indicates the value of the $T = 0$ K rate constant implied by that barrier.

Figures 3–7 compare the experimental rate constants for these systems (solid points) with values calculated from the potential barriers listed in the tables. All of these results correspond to one of the two limiting cases in which either all of the vibrational energy of the bond being broken contributes to motion along the reaction path, $E_0 = \epsilon_0$ (upper half of each table and solid curves in Figures 3–8), or when none of it does, $E_0 = 0$ (lower half of each table and dashed curves in Figures 3–8). Three-parameter fits in which $E_0$, $V_1$, and $a_1$ were all varied simultaneously in general converged to results which were statistically indistinguishable from those for the one of these limiting cases for which $\sigma$ is smallest.

In addition to the above, two-parameter fits were performed in which $E_0$ was fixed equal to either zero or to the appropriate $\epsilon_0$ value taken from Table I and $\bar{\nu}$ was fixed at the Table I value, while the frequency factor $A$ was set equal to trial values differing from this $\bar{\nu}$ by factors ranging from $10^{-4}$ to $10^4$. For all five systems, these changes *by eight orders of magnitude* in the assumed value of $A$ led to fitted $V_1$ values differing by up to 40% from the corresponding values in Tables II–VI, *but had virtually no effect on either the quality of fit* (i.e., the $\sigma$ value) or on the fitted value of the width parameter $a_1$! This shows that the parameters $A$ and $V_1$ of both the present and the "traditional" models are completely correlated when the data analyzed all describe the reaction of a single isotopic species, and it illustrates the ambiguity which could arise if $A$ were a free parameter which had to be determined from the analysis.

The above demonstration of the correlation between $A$ and $V_1$ raises serious doubts about the claim in ref 13 and 23 that unique values of $A$, $V_1$, and $a_1$ could be obtained from fits of eq 4 to the rate data for one isotopic form of an intramolecular H-atom transfer reaction.[49] At the same time, it seems clear that the simultaneous changes in $A$ and $V_1$ whose effects on the calculated rate constants exactly cancel one another for an H-atom transfer reaction will *not* cancel each other's effect on the rate constants for the analogous D-atom abstraction. Thus, for intramolecular hydrogen atom transfer in large molecules where the most appropriate value of $A$ is not readily apparent, it should be possible to determine a unique value of this quantity from a simultaneous fit to the rate constants for both isotopes.[50,51]

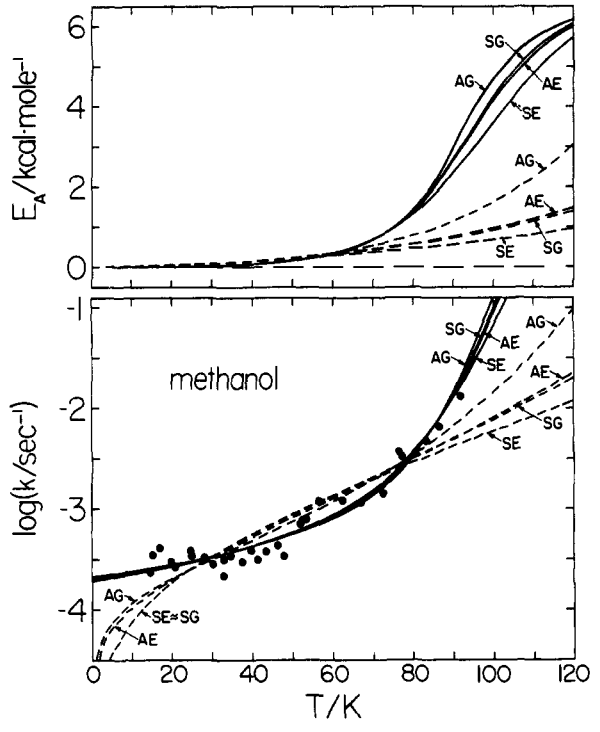


Figure 3. Lower: for H abstraction by $\cdot CH_3$ in methanol glass, comparison of experiment (solid points) with theoretical rate constants calculated from the barrier parameters in Table II for both $E_0 = \epsilon_0$ (solid curves) and $E_0 = 0$ (dashed curves) versions of the model. Upper: activation energies calculated for the same barrier parameters and $E_0$ values.

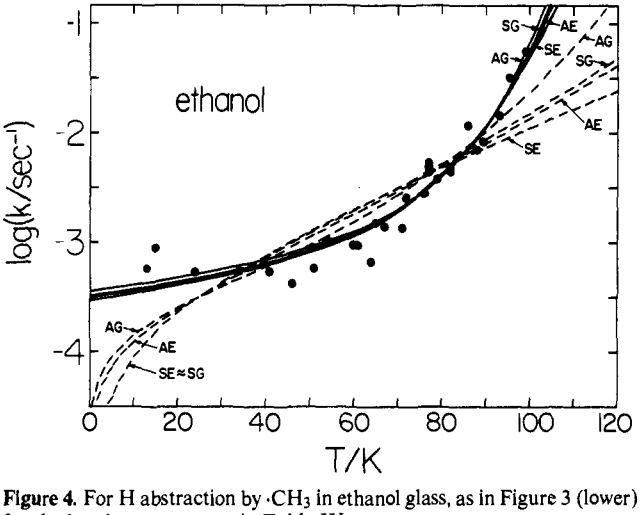


Figure 4. For H abstraction by $\cdot CH_3$ in ethanol glass, as in Figure 3 (lower) for the barrier parameters in Table III.

The curves in Figures 3–7 clearly illustrate the way tunneling-model rate constants depend on the functional form of the potential-energy barrier. In particular, the fact that Gaussian barriers are relatively narrower at the base than are equivalent Eckart barriers explains the slightly larger low-temperature rate constants associated with the former. Similarly, the fact that asymmetric barriers are relatively narrower at the base than are equivalent symmetric barriers explains the enhanced low-temperature rate constants for the former seen in these figures (and previously noted in ref 17). However, for cases in which the experimental rate constants are clearly approaching a finite limit at 0 K, these barrier-shape effects alone are much too small to properly simulate the observed behavior (e.g., see the dashed curves in Figures 3 and 4).

While the rate constants themselves are the fundamental experimental observable, the behavior of the apparent activation energy $E_A$ is often invoked in discussions of the characteristic properties of these low-temperature rate constants. The upper segments of Figures 3 and 6 therefore show how the calculated (from eq 9) values of $E_A$ vary with temperature for the various cases summarized in the tables. The analogous plots for the ethanol reaction are very similar to those seen in Figure 3, while those for acetonitrile II and methyl isocyanide are very similar to the curves in Figure 5. Note that in all cases these $E_A$ curves will asymptotically approach the constant value $[V_1 - E_0]$ at high temperatures.

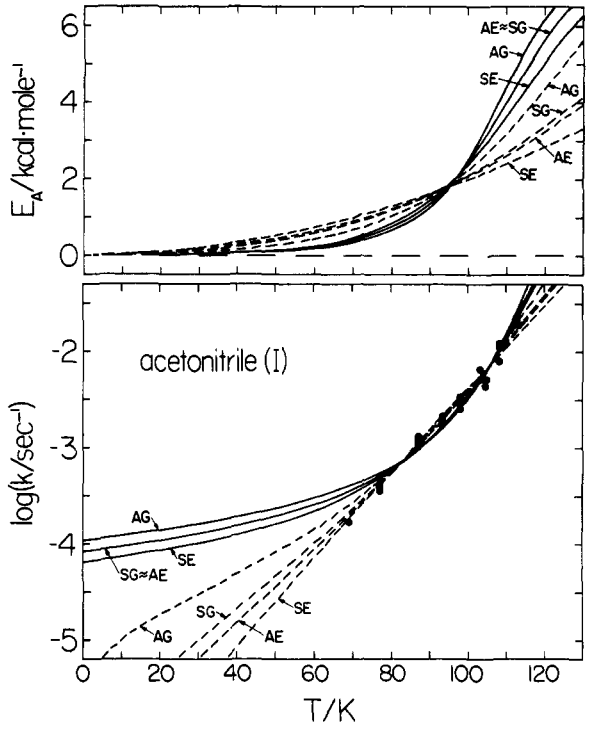


Figure 5. For H abstraction by $\cdot CH_3$ in crystal I acetonitrile, as in Figure 3 for the barrier parameters in Table IV.

**Importance of Nonnegligible Effective Zero-Point Energy $E_0$.** When comparing the $E_0 = \epsilon_0$ and $E_0 = 0$ results in Tables II–VI, the implications of the model dependence of the potential barrier parameters yielded by the fits must be considered. Since the barrier width parameter $a_1$ has a slightly different meaning for each of the four different potential forms, the values of it obtained from fits to a given set of data are not expected to be identical. However, the fact that the barrier height is directly related to the limiting high-temperature behavior of the observable (the rate constant) means that, for any reasonable model of the reaction, the derived barrier height $V_1$ should not depend significantly on the functional form chosen for the potential.

It is clear from the broad temperature range spanned by the experimental measurements that the methanol and ethanol systems provide the most stringent tests of the present model. For these reactions, the agreement with experiment seen in Figures 3 and 4 and the relative sizes of the $\sigma$ values in Tables II and III unambiguously affirm that the $E_0 = \epsilon_0$ version of the model is in much closer agreement with experiment than is that based on the assumption that $E_0 = 0$. Independent confirmation of the appropriateness of this model is provided by the fact that for both systems, the $V_1$ values obtained from the four $E_0 = \epsilon_0$ fits summarized in each of Tables II and III are virtually identical, while those corresponding to $E_0 = 0$ differ by up to a factor of 3. As a further test of this model dependence, these fits were repeated using symmetric and asymmetric Lorentzian potential energy barriers[52] which are typically much broader at the base than the exponential-tailed

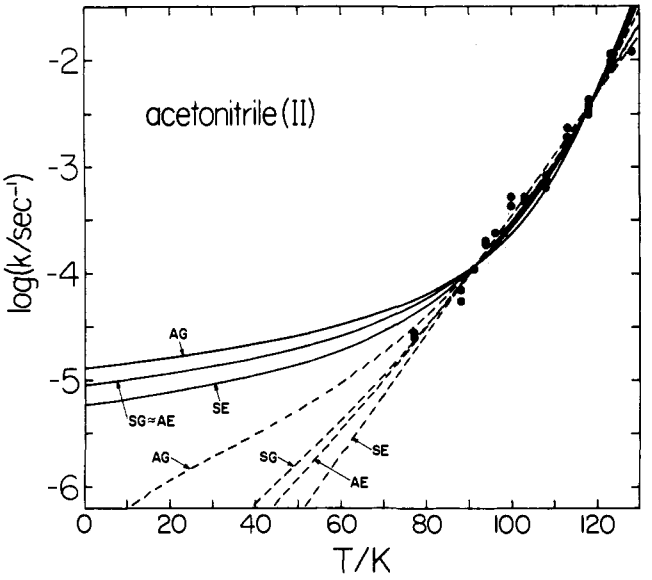


**Figure 6.** For H abstraction by $\cdot CH_3$ in crystal II acetonitrile, as in Figure 3 (lower) for the barrier parameters in Table V.

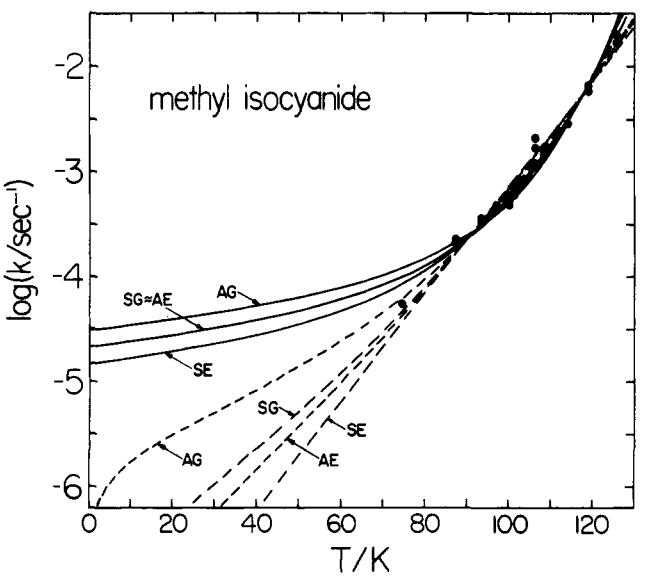


**Figure 7.** For H abstraction by $\cdot CH_3$ in crystalline methyl isocyanide, as in Figure 3 (lower) for the barrier parameters in Table VI.

Eckart or Gaussian barriers. While these $E_0 = \epsilon_0$ fits yielded $V_1$ values some 1-2 kcal/mol larger than those seen in Tables II and III, this difference is still negligible in comparison with the differences among the $V_1$ values obtained from the various $E_0 = 0$ fits. In contrast, $E_0 = 0$ fits to Lorentzian barriers had very much larger $\sigma$ values and the corresponding $V_1$ values were >80 kcal/mol.

For the acetonitrile and methyl isocyanide reactions the situation is much more ambiguous in that comparison of the various $\sigma$ values suggests that the $E_0 = 0$ fits should be preferred while the model dependence of the fitted $V_1$ values still favors $E_0 = \epsilon_0$ (though not so dramatically as for the alcohol systems). Firm conclusions are difficult to reach here because the temperature ranges spanned by these data are much narrower and do not include the very low temperatures at which the alcohol reactions were studied. However, Figures 5-7 show that the differences between the $\sigma$ values for these two sets of fits are largely due to the differences between their agreement with the experimental data at the lowest available temperatures. Owing to their relative magnitude, these are the measured rate constants which are expected to be least reliable. The types of fits reported in Tables IV-VI were therefore repeated with the experimental data at the very lowest temperature omitted from the analysis. In all cases, the resulting barrier parameters were very similar to those shown in the tables, but the differences between the $\sigma$ values for the $E_0 = \epsilon_0$ and $E_0 = 0$ cases were markedly reduced; indeed, for methyl isocyanide the two sets of $\sigma$ values become virtually the same. Moreover, three-parameter fits to these slightly truncated data sets ($N_d$ = 34, 29, and 17 for acetonitrile I, acetonitrile II, and methyl isocyanide, respectively) converged on $E_0$ values which, though distinctly smaller than $\epsilon_0$, were distinctly larger than zero.

One final point which bears on this argument concerns the size of the fitted $V_1$ values relative to the $E_A$ values for the analogous gas-phase reactions (see Table I). In the course of a gas-phase reaction the reagent particles are free to move so as to minimize the overall potential energy while the reagent C-H bond is stretching toward its breaking point. As a result, the observed gas-phase activation energy should be associated with the barrier height along the minimum-energy path on the full potential energy surface. In contrast, the reagents in the solid-phase abstraction are held at fixed positions, effectively defined by the van der Waals radius of the molecules of the host matrix, so they *may not* move to minimize the overall potential energy as the reaction proceeds. As a result, the barrier height

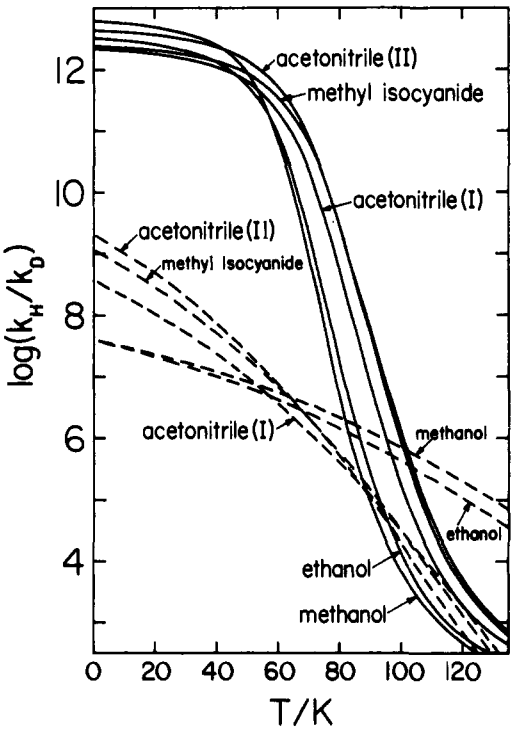


**Figure 8.** Isotopic rate constant ratios predicted from the $E_0 = \epsilon_0$ fits (solid curves) and $E_0 = 0$ fits (dashed curves) for the asymmetric Eckart (AE) barriers in Tables II-VI.

to reaction in the solid is expected to be somewhat higher than the activation energy for the analogous gas-phase reaction.[53] The results in Tables II-V show that this is true for all barriers obtained from $E_0 = \epsilon_0$ fits to the solid-phase alcohol and acetonitrile rate constants, but not true for some of the $E_0 = 0$ barriers. This observation therefore further discriminates against the appropriateness of the latter model for the acetonitrile and methyl isocyanide reactions.

## Conclusions

The quantitative agreement with a wide variety of experimental results shown by Figures 3-7 and Tables II-VI provides a convincing demonstration of the usefulness of the present model. The simple and internally consistent picture of the reactions which it provides contrasts strongly with the somewhat

ad hoc assumptions of the "traditional" approach. Moreover, the energy partitioning which is at the core of the present approach implicitly allows for either a finite reaction rate constant of $\bar{\nu}P(E_0)$ at 0 K or for the $k(0\text{ K}) = 0$ behavior predicted by the traditional approach. It seems clear that the $E_0 = \epsilon_0$, or at least $E_0$ significantly greater than zero, version of the present model provides the most satisfactory overall explanation of the data for the five systems considered here. This conclusion is certainly significantly weaker for the acetonitrile and methyl isocyanide reactions than for the abstractions from methanol and ethanol, and its unambiguous confirmation for those systems clearly awaits new lower temperature measurements. However, the quality of the agreement found here, combined with the simplicity and internal consistency of the theory, suggests that the present way of incorporating zero-point energy effects into the theory of tunneling-dominated reactions in low-temperature solids is essentially correct.

In view of the above and of the known exothermicity of the reactions for the first four cases considered, the potential-energy barriers for these five reactions are probably best represented by the asymmetric Eckart and asymmetric Gaussian functions (AE and AG). However, there are no grounds for choosing between these functions or indeed, on the basis of their ability to fit the data, even between them and their symmetric counterparts. Thus, although the trends seen in Figures 3-7 suggest that higher temperature measurements should be able to discriminate between them, present predictions based on either the AE or AG functions for these systems must be deemed equally reliable.

For all five reactions, Figure 8 shows the temperature dependence of the ratio of the calculated rate constants for H-atom and D-atom abstraction implied by the asymmetric Eckart barriers for $E_0 = \epsilon_0$ fits (solid curves) and $E_0 = 0$ fits (dashed curves). The dramatic difference between the isotope effects for these two versions of the model would appear to be an ideal way for discriminating between them, except for the fact that over this whole temperature range the D-atom transfer rates are too slow to be measured reliably using present techniques. Thus, the present predictions of isotope effects of magnitude $10^{12}$ may be rather difficult to test.

Listings of the computer program used for calculating the theoretical rate constants and fitting them to experimental data may be obtained from the first author (R.J.L.).

**Supplementary Material Available:** Tables of rate constants for hydrogen atom abstraction by methyl radicals (5 pages). Ordering information is given on any current masthead page.

## Refernces and Notes

(1) Research supported by the National Sciences and Engineering Research Council of Canada and by the Division of Chemical Sciences, Office of Basic Energy Sciences, U.S. Department of Energy (Document No. ORO-2968-117).
(2) University of Waterloo; John Simon Guggenheim Fellow, 1979–1980. Address until Aug 1980: Theoretical Chemistry Department, Oxford OX1 3TG, England.
(3) University of Tennessee.
(4) Department of Chemistry, University of Alberta, Edmonton, Alberta, Canada T6G 2G2.
(5) R. P. Bell, *Proc. R. Soc. London, Ser. A*, **148**, 241 (1935).
(6) S. Glasstone, K. J. Laidler, and H. Eyring, "The Theory of Rate Processes", McGraw-Hill, New York, 1941.
(7) E. D. Sprague and F. Williams, *J. Am. Chem. Soc.*, **93**, 787 (1971).
(8) O. Ye. Yakimchenko and Ya. S. Lebedev, *Int. J. Radiat. Phys. Chem.*, **3**, 17 (1971).
(9) R. J. Le Roy, E. D. Sprague, and F. Williams, *J. Phys. Chem.*, **76**, 546 (1972).
(10) J.-T. Wang and F. Williams, *J. Am. Chem. Soc.*, **94**, 2930 (1972).
(11) A. Campion and F. Williams, *J. Am. Chem. Soc.*, **94**, 7633 (1972).
(12) A. M. Dubinskaya and P. Yu. Butyagin, *Dokl. Akad. Nauk SSSR*, **211**, 141 (1973).
(13) G. Brunton, D. Griller, L. R. C. Barclay, and K. U. Ingold, *J. Am. Chem. Soc.*, **98**, 6803 (1976).
(14) E. D. Sprague, *J. Phys. Chem.*, **81**, 516 (1977).
(15) M. Iwasaki, K. Toriyama, K. Nunome, M. Fukaya, and H. Muto, *J. Phys. Chem.*, **81**, 1410 (1977).
(16) M. Iwasaki, K. Toriyama, H. Muto, and K. Nunome, *Chem. Phys. Lett.*, **56**, 494 (1978).
(17) K. Toriyama and M. Iwasaki, *J. Phys. Chem.*, **82**, 2056 (1978).
(18) M. H. J. Wijnen, *J. Chem. Phys.*, **22**, 1074 (1954).
(19) V. I. Goldanskii, M. D. Frank-Kamenetskii, and I. M. Barkalov, *Dokl. Adad. Nauk SSSR*, **211**, 133 (1973); *Science*, **182**, 1344 (1973).
(20) N. Alberding, R. H. Austin, K. W. Beeson, S. S. Chan, L. Eisenstein, H. Frauenfelder, and T. M. Nordlund, *Science*, **192**, 1002 (1976).
(21) R. L. Hudson, M. Shiotani, and F. Williams, *Chem. Phys. Lett.*, **48**, 193 (1977).
(22) K. Toriyama, K. Nunome, and M. Iwasaki, *J. Am. Chem. Soc.*, **99**, 5823 (1977).
(23) G. Brunton, J. A. Gray, D. Griller, L. R. C. Barclay, and K. U. Ingold, *J. Am. Chem. Soc.*, **100**, 4197 (1978).
(24) R. J. Le Roy, K. A. Quickert, and D. J. Le Roy, *Trans. Faraday Soc.*, **66**, 2997 (1970).
(25) C. Eckart, *Phys. Rev.*, **35**, 1303 (1930).
(26) H. Murai, unpublished work, 1978.
(27) One possible function of this type is $V(x) = A(x^2 - x_0^2)^2$, for $|x| \leq x_0$; $V(x) = 0$ for $|x| > x_0$.
(28) V. I. Goldanskii, *Dokl. Akad. Nauk SSSR*, **127**, 1037 (1959).
(29) P. H. Cribb, S. Nordholm, and N. S. Hush, *Chem. Phys.*, **29**, 43 (1978).
(30) Throughout this paper, log refers to the common logarithm (base 10) and ln to the Naperian logarithm (base *e*).
(31) As an alternative to Figure 1b, a plot of log ($k$) vs. $(T)^{1/2}$ might be considered.
(32) H. S. Johnston and D. Rapp, *J. Am. Chem. Soc.*, **83**, 1 (1961).
(33) E. M. Mortensen and K. S. Pitzer, *Chem. Soc., Spec. Publ.*, **No. 16**, 57 (1962).
(34) I. Shavitt, *J. Chem. Phys.*, **49**, 4048 (1968).
(35) M. D. Harmony, *Chem. Soc. Rev.*, **1**, 211 (1972).
(36) R. P. Bell, "The Proton in Chemistry," 2nd ed., Chapman and Hall, London, 1973.
(37) E. Caldin and V. Gold, Eds., "Proton-Transfer Reactions," Chapman and Hall, London, 1975.
(38) This is the same specific rate constant which appears in the semiclassical theory of the rotational predissociation of quasi-bound levels of a diatomic molecule; see, e.g., M.S. Child, *Spec. Period. Rep.: Mol. Spectrosc.*, **2**, 466 (1974).
(39) Of course, for transfer of different atomic isotopes via a given chemical reaction, $\bar{\nu}$ (and $A$), $\epsilon_0$, and $E_0$ all scale as $(m_a)^{-1/2}$, where $m_a$ is the mass of the atom being transferred.
(40) N. R. Draper and H. Smith, "Applied Regression Analysis", Wiley, New York, 1966.
(41) J. E. Willard, *Int. J. Radiat. Phys. Chem.*, **6**, 325 (1974).
(42) W. E. Putnam, D. M. McEachern, Jr., and J. E. Kilpatrick, *J. Chem. Phys.*, **42**, 749 (1965).
(43) (a) M. A. Bonin, Y. J. Chung, E. D. Sprague, K. Takeda, J. T. Wang, and F. Williams, *Nobel Symp.*, **22**, 103 (1973), and references cited therein; (b) T. Gillbro, K. Takeda, and F. Williams, *J. Chem. Soc., Faraday Trans. 2*, **70**, 465 (1974).
(44) E. D. Sprague, K. Takeda, J. T. Wang, and F. Williams, *Can. J. Chem.*, **52**, 2840 (1974).
(45) E. D. Sprague and F. Williams, *Acc. Chem. Res.*, in preparation.
(46) J. T. Wang, Ph.D. Thesis, University of Tennessee, 1972.
(47) (a) H. L. Holloman, M.S. Thesis, University of Tennessee, 1970; (b) E. D. Sprague, Ph.D. Thesis, University of Tennessee, 1971; (c) K. Takahashi, M.S. Thesis, University of Tennessee, 1972; (d) J. D. Skelton, unpublished work.
(48) A. A. Frost and R. G. Pearson, "Kinetics and Mechanism," 2nd ed., Wiley, New York, 1961, p 160.
(49) This high correlation between $A$ and $V_1$ was also observed in the results of fits to the H-atom data of Brunton et al.[13,23] which used either the $E_0 = 0$ or the $E_0 = \epsilon_0$ versions of the present model.[50]
(50) R. J. Le Roy, unpublished work, 1979.
(51) Assuming, of course, that the transition state is the same for the two isotopes.
(52) A Lorentzian potential barrier is defined by $V(x) = V_1/[1 + (x/a_1)^2]$, for $x \leq 0$, and $V(x) = V_2/[1 + (x/a_2)^2] - (V_2 - V_1)$, for $x > 0$, where continuity of the second derivative at $x = 0$ requires that $a_2 = a_1\sqrt{V_2/V_1}$.
(53) Note that in the gas-phase reaction the zero-point energy of the C–H stretch does not contribute directly to motion along the reaction path, so that $E_A$ (gas phase) is the analogue of our barrier height $V_1$.